Chemical Engineering Journal 453 (2023) 139958

Contents lists available at ScienceDirect

Chemical Engineering Journal

journal homepage: www.elsevier.com/locate/cej

A novel strategy for rapid identification of pyrolytic synergy and prediction of product yield: Insight into co-pyrolysis of xylan and polyethylene

Shengyu Xie [a], Shogo Kumagai [a,b,*], Naomichi Takahashi [a], Tomohito Kameda [a], Yuko Saito [a], Toshiaki Yoshioka [a]

[a] Graduate School of Environmental Studies, Tohoku University, 6-6-07 Aoba, Aramaki-aza, Aoba-ku, Sendai, Miyagi 980-8579, Japan
[b] Division for the Establishment of Frontier Sciences of Organization for Advanced Studies, Tohoku University, 2-1-1 Katahira, Aoba-ku, Sendai 980-8577, Japan

ARTICLE INFO

Keywords:
Xylan
Polyethylene
Pyrolytic interaction
Hierarchical clustering analysis
Response surface methodology

ABSTRACT

The distributions of biomass and plastic co-pyrolysis products are complicated by abundant component combinations, pyrolysis conditions, and synergies. Herein, the hierarchical clustering analysis (HCA) and response surface methodology (RSM) were used to rapidly determine synergies and predict product yields of xylan and polyethylene (PE) co-pyrolysis at 500–700 °C. The results showed that co-pyrolysis promoted liquid production and suppressed solid and char formation. Pyrolytic interactions improved the decomposition of the PE-derived wax, resulting in 1.5–1.9- and 1.7–2.1-fold higher yields of heavy gas oil and $C_{\geq 26}$ hydrocarbons compared to the theoretical values. HCA classified pyrolyzates with similar synergy into the same cluster, which reflected the suppressed carbonyl compound production, enhanced furfural and phenols yields at 700 °C, and greater C_{17}–C_{30} hydrocarbon production. The quadratic model of RSM predicted the yields of gas, CO, C_3H_n, C_4H_n, liquid, ethanol, acetaldehyde, hydrocarbon oil, gasoline, solid, and char influenced by synergies. Owing to complex interactions, the cubic model fitted the CH_4 and C_2H_4 yields. The linear model described the CO_2 yield without synergy. This work illustrates the utility of combining RSM and HCA to predict product distributions of various waste co-treatment processes.

1. Introduction

Renewable lignocellulosic biomass can relieve the energy crisis and carbon emission pressure induced by the excessive use of fossil fuels. Approximately 12,000 million tons of plastic waste will be in the landfills or natural environment by 2050, causing severe pollution and wasting petroleum resources [1]. Furthermore, the massive demand for woody and plastic composite materials in decking and construction fields has exacerbated the pressure associated with the disposal of the biomass and plastic wastes [2]. These hard-to-separate wastes have to be treated using landfills and incineration, which complicates achieving the targets of the circular economy and carbon neutrality.

Pyrolysis is widely used to recover valuable chemicals and fuels from the hard-to-recycle polymeric materials [3–5]. Notably, co-pyrolysis offers a convenient treatment of mixtures that does not require additional physical separation [6–8]. In general, the oxygen content of the biomass oil is over 10-fold higher than that of petroleum, which explains low heating value, poor thermal stability, and high corrosivity of the biomass oil [9]. Plastic blending improves the biomass oil quality by increasing the hydrogen-to-carbon effective ratio [10,11]. Furthermore, the suppression of coke formation by hydrogen-rich reactants during pyrolysis enhances the efficiency of biomass carbon conversion to chemicals [12].

The positive impacts of biomass-plastic synergies on product recovery have been reported and summarized previously [13–17]. Polyethylene (PE) and polypropylene account for a half of the total plastic waste production and have hydrogen content of 14 wt%. Therefore, their pyrolyzates can provide hydrogen donors to hydrogen-deficient biomass during pyrolysis [18,19]. A previous study found that PE increased the yields of furans, acids, and methyl or propenyl phenols during red oak pyrolysis [20]. Furthermore, the breakdown of PE into aliphatic compounds with lower numbers of carbons was promoted by the hydroxyl intermediates of sugarcane bagasse pyrolysis [21]. Previous works identified the liquid/solid- and gas phase synergies during the biomass and polyolefin co-pyrolysis to improve the recovery of levoglucosan, methoxyphenol, and hydrocarbon oil [22–25].

* Corresponding author at: Graduate School of Environmental Studies, Tohoku University, 6-6-07 Aoba, Aramaki-aza, Aoba-ku, Sendai, Miyagi 980-8579, Japan.
E-mail address: kumagai@tohoku.ac.jp (S. Kumagai).

https://doi.org/10.1016/j.cej.2022.139958
Received 20 July 2022; Received in revised form 13 October 2022; Accepted 18 October 2022
Available online 22 October 2022

Pyrolysis of xylan, the main hemicellulose component of hardwoods, can be used to produce acids, aldehydes, and furfural chemicals [26–28]. Synergies of the xylan and plastic co-pyrolysis received less attention than synergies of the biomass and plastic co-pyrolysis. Pyrolysis-gas chromatography/mass spectrometry (Py-GC/MS) showed that synergies between xylan and PE enhanced alkene production, although the furan and saccharide yields decreased [29]. In addition, catalyzed co-pyrolysis of xylan and polyolefin improved the aromatic compound production [30,31]. However, co-pyrolysis of xylan and plastic needs to be further studied to understand the pyrolyzate yields of co-pyrolysis and determine the possibility of future industrial applications.

Currently, numerous pyrolyzates generated during polymer pyrolysis complicate identification of pyrolytic synergies. The complex product distribution is influenced by various combinations of the plastic, biomass, and co-pyrolysis conditions. Response surface methodology (RSM) has been successfully applied to predict pyrolyzate yields and reveal synergies based on the polynomial models fitted to the experimental data [32]. Nevertheless, it is difficult to establish accurate RSM models for pyrolyzates with a low yield, which precludes comprehensive evaluation of pyrolytic interactions. Hierarchical clustering analysis (HCA) can be used to compare large amounts of data and then conduct multiple classification analyses [33]. Therefore, HCA can be applied to classify numerous pyrolyzates with similar synergies into the same cluster, and this approach has been occasionally utilized in the pyrolysis [34], combustion [35], and gasification fields [36]. RSM constructs a more reasonable yield distribution model based on the HCA-identified interactions, and HCA effectively complements the deficiencies of RSM in evaluating co-pyrolysis synergies. Based on the above knowledge, we propose here a rapid approach to identify interactions and predict product yields by combining HCA and RSM, which has never been reported in the co-treatment process. This strategy is beneficial for the maximal utilization of the biomass and waste plastics to recover chemical feedstocks.

Herein, the product recovery test of xylan and PE co-pyrolysis was conducted in a tube reactor at 500–700 °C with different PE blending proportions. HCA was applied to rapidly analyze the subtle synergies during co-pyrolysis. The distribution models of major pyrolyzates were established by RSM to predict product yields for various experimental conditions.

2. Materials and methods

2.1. Materials

Xylan isolated from beech wood and high-density PE (average M_w = 150,000) were obtained from Serva Electrophoresis GmbH company (Heidelberg, Germany) and the Japanese domestic market, respectively. Xylan was demineralized by washing with 0.05 M HCl/methanol for 24 h twice at room temperature [28]. By using an elemental analyzer (JM10, J-Science Lab, Japan), it was found that xylan contained 44.2 wt % C, 6.3 wt% H, and 48.5 wt% O. The prepared materials were ground and sieved to powders with a particle diameter below 75 μm. Before the experiments, the samples were dried at 105 °C overnight to remove moisture. Powders containing xylan and PE at different blending proportions were placed in a microtube and shaken for 5 min to obtain homogenous mixtures. Chemicals used in the experiments were purchased from Kanto Chemical (Tokyo, Japan) or Tokyo Chemical Industry (Tokyo, Japan). Standard gases were from Tanuma Sanso Shokai (Sendai, Japan).

2.2. RSM design

The central composite design was applied to determine the co-pyrolysis conditions by utilizing Stat-Ease 360 software (Stat-Ease Inc., Minneapolis, MN, USA), including central points (600 °C, 50 wt%), axial points (500 and 700 °C, 0 and 100 wt%), and factorial points (530 and 670 °C, 15 and 85 wt%), as shown in Fig. S1 in the electronic supplementary information (ESI). The condition design of five levels for each factor can effectively reflect the pyrolytic interaction with the minimal number of experiments [32]. The polynomial equations containing various terms (Eq. (1)) were selected to fit experimental results until the most suitable model was obtained according to the analysis of variance (ANOVA):

$$Y=\beta_0+\beta_1A+\beta_2B+\beta_{12}AB+\beta_{11}A^2+\beta_{22}B^2+\beta_{122}AB^2+\beta_{112}A^2B+\beta_{111}A^3+\beta_{222}B^3 \quad (1)$$

where Y represents pyrolyzate yield; A and B represent pyrolysis temperature and PE blending ratio, respectively; whereas other symbols are the intercept (β_0), linear (β_1 and β_2), quadratic (β_{12}, β_{11}, and β_{22}), and cubic (β_{122}, β_{112}, β_{111}, and β_{222}) interaction coefficients of the model, respectively. The influence of a term was considered statistically significant if ANOVA P-value was below 0.05. The detailed information is provided in ESI.

2.3. Pyrolysis experiments in a tube reactor

The pyrolysis experiments were performed in a quartz tube reactor (inner diameter of 7 mm) heated by an electric furnace (Fig. S2a). A sample (0.1 g) was placed outside the heating zone and fixed by quartz wools. Helium (>99.9999 % purity) was swept at 50 mL/min into the whole apparatus during experiments to create an inert environment and carry the pyrolyzates. When the furnace was heated to a preset temperature, it was moved to the position where the sample was located at the center of the heating zone. After the sample was heated for 15 min, the furnace heating was terminated, the quartz tube was naturally cooled to 50 °C by the continued helium flow, and then, the cold trap was defrosted for transferring the condensed gases into the aluminum bag. Char remained in the heating zone of the quartz tube, and the liquid/solid was condensed outside of the heating zone. Therefore, the quartz tube was cut into two sections for weight measurement (Fig. S2b). Lastly, each part of the apparatus was separated and weighed, respectively. The liquid products were collected in the eluate after washing the cut tube, joint, and trap with 10 mL of super-dehydrated tetrahydrofuran (THF). All pyrolysis experiments were repeated at least twice to ensure the reproducibility of the results.

2.4. Product analysis

The total gas yield is the sum of H_2 and C_{1-4} gas yields. Specific gases were quantified by GC with a thermal conductivity detector and flame ionization detection. The liquid yield was the total sum of weight differences of the cut tube, joint, and trap before and after washing with 10 mL of THF. The liquid products were identified and quantified by GC/MS/flame ionization detection. The details of the GC system condition are listed in Tables S1 and S2. The products except for aliphatic hydrocarbon were identified based on the NIST 17 library, which had > 80 % of match factors. The high-boiling-point hydrocarbons dissolved in THF in the tube reactor test had low GC/MS intensity responses and match degrees; thus, they were identified after referring to online Py-GC/MS results under the same condition. Furthermore, the water content of the liquid was determined by the Karl Fischer titration. Xylan-derived coke and PE-derived wax (defined as solid) were deposited in the same position, and the yield was determined by the weight difference of the THF-rinsed cut tube before and after combustion at 900 °C. The remained char in the cut tube was calculated based on the weight difference of the cut tube before and after combustion at 900 °C.

The yield difference (YD) was used to identify the pyrolytic interaction, which was calculated using the following equations:

$$Y_{mixture\_cal} = (1 - B)Y_{xylan} + BY_{PE} \quad (2)$$

Table 1
Weight compositions of identified pyrolyzates from xylan, PE, and mixtures under RSM designed conditions.

	500–0 [a]	500–50	500–100	530–15	530–85	600–0	600–50	600–100	670–15	670–85	700–0	700–50	700–100
Gas (wt%)	**13.6 ± 0.1**	**8.0 ± 0.0**	**2.3 ± 0.0**	**12.1 ± 0.0**	**4.2 ± 0.0**	**14.4 ± 0.3**	**8.6 ± 0.2**	**3.1 ± 0.1**	**13.2 ± 0.1**	**5.2 ± 0.0**	**16.2 ± 0.0**	**9.4 ± 0.3**	**4.5 ± 0.1**
H_2	– [c]	–	–	–	–	0.1 ± 0.0	+	–	0.2 ± 0.0	+	0.3 ± 0.1	0.2 ± 0.0	–
CO	2.7 ± 0.0 [d]	1.4 ± 0.0	–	2.4 ± 0.0	0.4 ± 0.0	3.1 ± 0.1	1.5 ± 0.1	–	3.0 ± 0.0	0.6 ± 0.0	4.3 ± 0.1	1.9 ± 0.0	–
CO_2	10.2 ± 0.1	5.1 ± 0.0	–	8.7 ± 0.0	1.4 ± 0.0	10.3 ± 0.1	5.1 ± 0.1	–	8.8 ± 0.0	1.4 ± 0.1	10.6 ± 0.0	5.1 ± 0.3	–
CH_4	0.4 ± 0.0	0.2 ± 0.0	0.1 ± 0.0	0.4 ± 0.0	0.1 ± 0.0	0.5 ± 0.0	0.3 ± 0.0	0.1 ± 0.0	0.5 ± 0.0	0.2 ± 0.0	0.6 ± 0.0	0.3 ± 0.0	0.2 ± 0.0
C_2H_4	0.1 ± 0.0	0.2 ± 0.0	0.3 ± 0.0	0.1 ± 0.0	0.4 ± 0.0	0.1 ± 0.0	0.3 ± 0.0	0.5 ± 0.0	0.1 ± 0.0	0.6 ± 0.0	0.1 ± 0.0	0.4 ± 0.0	1.0 ± 0.0
C_2H_6	0.1 ± 0.0	0.2 ± 0.0	0.2 ± 0.0	0.1 ± 0.0	0.2 ± 0.0	0.1 ± 0.0	0.2 ± 0.0	0.3 ± 0.0	0.1 ± 0.0	0.3 ± 0.0	0.1 ± 0.0	0.2 ± 0.0	0.4 ± 0.0
C_3 hydrocarbon	0.1 ± 0.0	0.5 ± 0.0	0.9 ± 0.0	0.2 ± 0.0	0.9 ± 0.0	0.1 ± 0.0	0.6 ± 0.0	1.1 ± 0.0	0.2 ± 0.0	1.1 ± 0.0	0.1 ± 0.0	0.7 ± 0.0	1.5 ± 0.0
C_4 hydrocarbon	0.1 ± 0.0	0.5 ± 0.0	0.8 ± 0.0	0.2 ± 0.0	0.8 ± 0.0	0.1 ± 0.0	0.5 ± 0.0	1.0 ± 0.0	0.2 ± 0.0	1.0 ± 0.0	0.1 ± 0.0	0.6 ± 0.0	1.4 ± 0.0
Liquid (wt%)	**51.5 ± 0.7**	**30.6 ± 0.5**	**9.2 ± 0.4**	**44.7 ± 1.5**	**15.2 ± 0.3**	**54.2 ± 1.6**	**33.5 ± 0.3**	**11.7 ± 0.0**	**54.3 ± 0.3**	**24.1 ± 0.2**	**55.8 ± 0.4**	**39.9 ± 0.9**	**19.2 ± 0.8**
C_2-C_3 carbonyl compounds	*2.8 ± 0.0*	*1.0 ± 0.2*	–	*1.9 ± 0.0*	*0.3 ± 0.1*	*2.6 ± 0.1*	*0.9 ± 0.1*	–	*1.6 ± 0.1*	*0.3 ± 0.0*	*2.5 ± 0.1*	*0.8 ± 0.1*	–
Acetaldehyde	1.1 ± 0.0	0.4 ± 0.1	–	0.8 ± 0.0	0.1 ± 0.0	0.9 ± 0.0	0.4 ± 0.1	–	0.7 ± 0.1	0.2 ± 0.0	0.8 ± 0.1	0.4 ± 0.1	–
Ethanol	1.6 ± 0.0	0.6 ± 0.1	–	1.0 ± 0.0	0.2 ± 0.0	1.5 ± 0.1	0.5 ± 0.0	–	0.8 ± 0.0	0.1 ± 0.0	1.5 ± 0.0	0.4 ± 0.0	–
Acetone	0.1 ± 0.0	0.1 + 0.0	–	0.1 + 0.0	+	0.1 ± 0.0	+	–	0.1 ± 0.0	0.1 + 0.0	0.1 ± 0.0	+	–
Propanoic acid	0.1 ± 0.0	+	–	+	+	0.1 ± 0.0	+	–	+	+	0.1 ± 0.0	+	–
5-membered-ring compounds	*0.3 ± 0.0*	*0.1 ± 0.0*	–	*0.3 ± 0.0*	+	*0.7 ± 0.1*	*0.2 ± 0.1*	–	*0.2 ± 0.0*	+	*0.5 ± 0.0*	*0.4 ± 0.0*	–
Furfural	0.2 ± 0.0	0.1 ± 0.0	–	0.3 ± 0.0	+	0.6 ± 0.1	0.2 ± 0.1	–	0.1 ± 0.0	+	0.5 ± 0.0	0.3 ± 0.0	–
2-Furanmethanol	+ [e]	+	–	+	+	+	+	–	+	+	+	+	–
2-Cyclopenten-1-one, 2-hydroxy	+	+	–	+	+	+	+	–	+	+	+	+	–
2-Cyclopenten-1-one, 2-methyl	+	+	–	+	+	+	+	–	+	+	+	+	–
Phenols	*0.1 ± 0.0*	+	–	*0.1 ± 0.0*	+	*0.1 ± 0.0*	+	–	*0.1 ± 0.0*	+	*0.1 ± 0.0*	+	–
Phenol	+	+	–	+	+	+	+	–	+	+	+	+	–
Phenol, methyl-	0.1 ± 0.0	+	–	0.1 ± 0.0	+	0.1 ± 0.0	+	–	+	+	+	+	–
Hydrocarbon oil	*0.3 ± 0.0*	*2.5 ± 0.3*	*4.1 ± 0.1*	*1.7 ± 0.1*	*4.3 ± 0.3*	*0.3 ± 0.0*	*4.5 ± 0.5*	*7.0 ± 0.4*	*2.1 ± 0.3*	*13.9 ± 0.2*	*0.2 ± 0.0*	*8.0 ± 0.7*	*14.0 ± 0.9*
Gasoline	*0.3 ± 0.0*	*0.8 ± 0.1*	*1.9 ± 0.1*	*0.5 ± 0.0*	*1.2 ± 0.1*	*0.3 ± 0.0*	*1.0 ± 0.3*	*2.5 ± 0.1*	*0.2 ± 0.0*	*2.2 ± 0.0*	*0.2 ± 0.0*	*1.9 ± 0.1*	*4.0 ± 0.2*
C_5	0.1 ± 0.0	0.4 ± 0.1	0.5 ± 0.0	0.3 ± 0.0	0.6 ± 0.1	0.1 ± 0.0	0.6 ± 0.1	0.7 ± 0.0	0.1 ± 0.0	1.1 ± 0.0	0.1 ± 0.0	1.0 ± 0.0	1.0 ± 0.0
C_6	0.1 ± 0.0	0.2 ± 0.0	0.8 ± 0.0	0.2 ± 0.0	0.3 ± 0.0	0.1 ± 0.0	0.3 ± 0.2	1.1 ± 0.0	0.1 ± 0.0	0.6 ± 0.0	+	0.6 ± 0.0	1.7 ± 0.0
C_7	0.1 ± 0.0	0.1 ± 0.0	0.4 ± 0.0	0.1 ± 0.0	0.2 ± 0.0	0.1 ± 0.0	0.1 ± 0.1	0.5 ± 0.0	+	0.3 ± 0.0	+	0.2 ± 0.0	0.8 ± 0.0
C_8	–	0.1 ± 0.0	0.2 ± 0.0	+	+	–	+	0.2 ± 0.1	+	0.1 + 0.0	–	+	0.3 ± 0.0
C_9	–	+	+	+	+	–	+	+	+	+	–	+	+
C_{10}	–	+	+	+	+	–	+	+	+	0.1 + 0.0	–	+	0.2 ± 0.1
Kerosene	–	*0.1 ± 0.0*	*0.1 ± 0.0*	*0.1 ± 0.0*	*0.2 ± 0.0*	–	*0.2 ± 0.1*	*0.8 ± 0.0*	*0.1 ± 0.0*	*2.0 ± 0.1*	–	*0.5 ± 0.1*	*1.7 ± 0.1*
C_{11}	–	+	+	+	+	–	+	0.2 ± 0.1	+	0.4 ± 0.0	–	0.1 ± 0.0	0.5 ± 0.0
C_{12}	–	+	+	+	+	–	+	0.1 ± 0.0	+	0.7 ± 0.0	–	0.2 ± 0.1	0.5 ± 0.2
C_{13}	–	0.1 ± 0.0	0.1 ± 0.0	0.1 ± 0.0	0.2 ± 0.0	–	0.2 ± 0.1	0.4 ± 0.0	0.1 ± 0.0	0.8 ± 0.0	–	0.3 ± 0.1	0.7 ± 0.0
Diesel	–	*0.7 ± 0.1*	*0.9 ± 0.1*	*0.4 ± 0.0*	*1.2 ± 0.0*	–	*1.5 ± 0.1*	*1.9 ± 0.0*	*0.4 ± 0.1*	*4.1 ± 0.2*	–	*1.9 ± 0.2*	*3.9 ± 0.7*
C_{14}	–	0.1 ± 0.0	0.2 ± 0.0	0.1 ± 0.0	0.3 ± 0.0	–	0.3 ± 0.1	0.5 ± 0.0	0.1 ± 0.0	1.0 ± 0.0	–	0.4 ± 0.1	0.9 ± 0.1
C_{15}	–	0.1 ± 0.0	0.2 ± 0.0	0.1 ± 0.0	0.3 ± 0.0	–	0.3 ± 0.0	0.5 ± 0.0	0.1 ± 0.0	0.9 ± 0.0	–	0.4 ± 0.0	0.9 ± 0.1

(*continued on next page*)

Table 1 (*continued*)

	500–0 [a]	500–50	500–100	530–15	530–85	600–0	600–50	600–100	670–15	670–85	700–0	700–50	700–100
C_{16}	–	0.1 ± 0.0	0.2 ± 0.0	0.1 ± 0.0	0.3 ± 0.0	–	0.3 ± 0.0	0.4 ± 0.0	0.1 ± 0.0	0.8 ± 0.0	–	0.4 ± 0.0	0.8 ± 0.1
C_{17}	–	0.1 ± 0.0	0.2 ± 0.0	0.1 ± 0.0	0.2 ± 0.0	–	0.3 ± 0.0	0.3 ± 0.0	0.1 ± 0.0	0.8 ± 0.0	–	0.4 ± 0.0	0.7 ± 0.1
C_{18}	–	0.1 ± 0.0	0.2 ± 0.0	0.1 ± 0.0	0.2 ± 0.0	–	0.3 ± 0.0	0.3 ± 0.0	0.1 ± 0.0	0.7 ± 0.0	–	0.4 ± 0.0	0.7 ± 0.1
Heavy gas oil	–	*0.7 ± 0.0*	*0.9 ± 0.1*	*0.5 ± 0.1*	*1.2 ± 0.1*	–	*1.3 ± 0.0*	*1.4 ± 0.1*	*0.8 ± 0.1*	*4.0 ± 0.0*	–	*2.5 ± 0.2*	*3.3 ± 0.5*
C_{19}	–	0.1 ± 0.0	0.1 ± 0.0	0.1 ± 0.0	0.2 ± 0.0	–	0.2 ± 0.0	0.2 ± 0.0	0.1 ± 0.0	0.7 ± 0.0	–	0.4 ± 0.0	0.6 ± 0.1
C_{20}	–	0.1 ± 0.0	0.1 ± 0.0	0.1 ± 0.0	0.2 ± 0.0	–	0.2 ± 0.0	0.2 ± 0.0	0.1 ± 0.0	0.6 ± 0.0	–	0.4 ± 0.0	0.5 ± 0.1
C_{21}	–	0.1 ± 0.0	0.1 ± 0.0	0.1 ± 0.0	0.2 ± 0.0	–	0.2 ± 0.0	0.2 ± 0.0	0.1 ± 0.0	0.6 ± 0.0	–	0.4 ± 0.0	0.5 ± 0.1
C_{22}	–	0.1 ± 0.0	0.1 ± 0.0	0.1 ± 0.0	0.2 ± 0.0	–	0.2 ± 0.0	0.2 ± 0.0	0.1 ± 0.0	0.6 ± 0.0	–	0.4 ± 0.0	0.5 ± 0.0
C_{23}	–	0.1 ± 0.0	0.1 ± 0.0	0.1 ± 0.0	0.2 ± 0.0	–	0.2 ± 0.0	0.2 ± 0.0	0.1 ± 0.0	0.5 ± 0.0	–	0.4 ± 0.0	0.4 ± 0.1
C_{24}	–	0.1 ± 0.0	0.1 ± 0.0	0.1 ± 0.0	0.2 ± 0.0	–	0.2 ± 0.0	0.2 ± 0.0	0.1 ± 0.0	0.5 ± 0.0	–	0.4 ± 0.0	0.4 ± 0.1
C_{25}	–	0.1 ± 0.0	0.1 ± 0.0	0.1 ± 0.0	0.1 ± 0.0	–	0.1 ± 0.0	0.2 ± 0.0	0.1 ± 0.0	0.5 ± 0.0	–	0.3 ± 0.0	0.4 ± 0.0
$C_{\geq 26}$ hydrocarbon	–	*0.3 ± 0.0*	*0.3 ± 0.0*	*0.2 ± 0.0*	*0.5 ± 0.1*	–	*0.5 ± 0.0*	*0.5 ± 0.1*	*0.5 ± 0.1*	*1.6 ± 0.0*	–	*1.2 ± 0.1*	*1.1 ± 0.0*
C_{26}	–	0.1 ± 0.0	0.1 ± 0.0	0.1 ± 0.0	0.1 ± 0.0	–	0.1 ± 0.0	0.1 ± 0.0	0.1 ± 0.0	0.4 ± 0.0	–	0.3 ± 0.0	0.3 ± 0.0
C_{27}	–	+	+	+	0.1 ± 0.0	–	0.1 ± 0.0	0.1 ± 0.0	0.1 ± 0.0	0.2 ± 0.0	–	0.2 ± 0.0	0.2 ± 0.0
C_{28}	–	+	0.1 ± 0.0	+	0.1 ± 0.0	–	0.1 ± 0.0	0.1 ± 0.0	0.1 ± 0.0	0.3 ± 0.0	–	0.2 ± 0.0	0.2 ± 0.0
C_{29}		0.1 ± 0.0	0.1 ± 0.0	0.1 ± 0.0	0.1 ± 0.0	–	0.1 ± 0.0	0.1 ± 0.0	0.1 ± 0.0	0.4 ± 0.0	–	0.3 ± 0.0	0.3 ± 0.0
C_{30}		0.1 ± 0.0	0.1 ± 0.0	0.1 ± 0.0	0.1 ± 0.0	–	0.1 ± 0.0	0.1 ± 0.0	0.1 ± 0.0	0.4 ± 0.0	–	0.3 ± 0.0	0.3 ± 0.0
Water	*18.3 ± 0.2*	*12.2 ± 0.4*	–	*17.6 ± 0.1*	*6.2 ± 1.4*	*21.0 ± 0.5*	*13.2 ± 0.6*	–	*19.3 ± 1.2*	*6.1 ± 0.0*	*21.8 ± 0.0*	*13.0 ± 0.2*	–
Others	*29.7 ± 0.9*	*14.7 ± 0.5*	*5.1 ± 0.5*	*23.2 ± 1.3*	*4.3 ± 1.3*	*29.4 ± 1.2*	*14.7 ± 0.8*	*4.7 ± 0.4*	*31.1 ± 1.2*	*3.7 ± 0.4*	*30.7 ± 0.4*	*17.7 ± 0.2*	*5.3 ± 0.1*
Solid (wt%)	**1.0 ± 0.2**	**41.0 ± 0.4**	**84.0 ± 0.4**	**14.9 ± 0.7**	**68.9 ± 0.5**	**1.0 ± 0.3**	**37.4 ± 1.1**	**80.8 ± 2.2**	**8.9 ± 0.1**	**59.7 ± 0.6**	**1.5 ± 0.1**	**32.2 ± 0.5**	**69.9 ± 2.6**
Char (wt%)	**24.3 ± 1.6**	**11.2 ± 0.0**	**–**	**19.9 ± 0.2**	**2.4 ± 0.1**	**22.0 ± 0.6**	**10.4 ± 0.5**	**–**	**14.1 ± 0.3**	**2.3 ± 0.1**	**18.4 ± 0.5**	**7.5 ± 0.0**	**–**
Total [b] (wt%)	**90.4 ± 1.2**	**90.9 ± 0.0**	**95.5 ± 0.7**	**91.7 ± 2.4**	**90.6 ± 0.2**	**91.6 ± 1.5**	**89.8 ± 0.7**	**95.6 ± 2.3**	**90.5 ± 0.0**	**91.3 ± 0.5**	**91.9 ± 0.2**	**89.0 ± 0.7**	**93.6 ± 1.9**

[a] *A-B*: *A* indicates pyrolysis temperature and *B* indicates PE proportion; [b] Total of gas, liquid, solid, and char; [c] Not detected; [d] Standard deviation<0.05; [e] Average value<0.05 wt%.

$$YD = Y_{mixture} / Y_{mixture\_cal} \quad (3)$$

where $Y_{mixture\_cal}$ corresponds to the theoretically calculated yield from co-pyrolysis; Y_{xylan} and Y_{PE} correspond to the experimental yields from neat xylan and PE pyrolysis, respectively; B corresponds to the PE blending proportion; $Y_{mixture}$ corresponds to the experimental yield from co-pyrolysis.

2.5. HCA of pyrolyzates

HCA was conducted using Origin 2021 software (OriginLab Corporation, Northampton, MA, USA). Euclidean distance is a classical similarity measure used for the analysis of continuous variables. Ward's linkage is based on finding the pair of clusters that leads to a minimum increase in the total within-cluster variance after merging [37], which can clearly differentiate cluster groups in this study. The HCA results are expressed by heat maps (matrix X ($m \times n$), where m represents pyrolyzates, and n represents pyrolysis conditions) combined with dendrograms, respectively.

3. Results and discussion

3.1. Pyrolysis of xylan, PE, and their mixtures

The identified pyrolyzate yields from the pyrolysis of xylan, PE, and their mixtures under different conditions are listed in Table 1. Increases in the gas yield (13.6 to 16.2 wt%) and liquid yield (51.5 to 55.8 wt%) as well as a decrease in the char yield (24.3 to 18.4 wt%) were observed with the rise in the xylan pyrolysis temperature from 500 to 700 °C. Xylan pyrolysis produced more gas and liquid and less solid yield than cellulose pyrolysis under the same conditions [32], which was related to the presence of short-chain heteropolysaccharides in xylan and its low polymerization. PE pyrolysis generated a large amount of solid consisting of high molecular weight wax. The liquid yield increased from 9.2 to 19.2 wt%, and the solid yield accordingly decreased from 84.0 to 69.9 wt% with the rise in PE pyrolysis temperature owing to the greater extent of depolymerization at high temperatures.

During co-pyrolysis, the yields of gas, liquid, and char increased, and the solid yield decreased when the mixture contained a higher xylan proportion. As shown by the thermogravimetric analysis (Fig. S3), fast co-pyrolysis of xylan and PE generated greater synergistic effects and weakened the thermal conductivity difference more than slow pyrolysis. Compared with the experimental and theoretically calculated values of

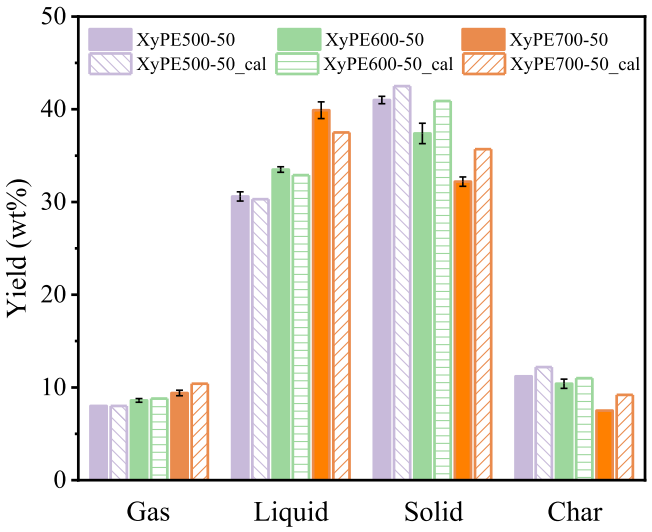

Fig. 1. Comparison of the experimental and theoretically calculated yields (_cal) of co-pyrolysis products (xylan:PE = 50:50, w/w) at different temperatures. Solid consists of high-molecular-weight compounds from xylan and PE-derived wax.

the product distribution (Fig. 1), co-pyrolysis of xylan and PE promoted liquid production and suppressed the formation of solid and char. Furthermore, these pyrolytic interactions were enhanced with the increase in temperature because the intense gas-phase interactions at high temperatures favored the breakdown of vapored intermediates during co-pyrolysis, resulting in the transformation of wax into liquid [22,38]. In addition, numerous H-donor species generated from polyolefin pyrolysis inhibited the cyclization and aromatization reactions leading to the formation of char [39].

CO and CO_2 were the major gaseous compounds generated by neat xylan pyrolysis (Table 1). The CO yield increased from 2.7 to 4.3 wt% with the rise in temperature. However, the CO_2 yield (10.2–10.6 wt%) was not significantly altered by changing the temperature. Such results may be explained as follows: CO is mainly generated from the aldehyde decarbonylation reactions, whereas CO_2 is derived from the primary decarboxylation reactions of the O-acetyl groups linked to xylan unit [26]. The CO_2 yield from xylan pyrolysis was far higher than our reported yield (2.7–3.0 wt%) from cellulose pyrolysis [32], because xylan contains more organic moieties with carboxyl content [40]. In addition, the yield of the C_2–C_4 hydrocarbons, main gaseous compounds generated by PE pyrolysis, significantly increased with the rise in temperature.

The CO and CO_2 yields were decreased and the C_2–C_4 hydrocarbon yield was increased by adding more PE during co-pyrolysis. The influence of pyrolytic interactions on gaseous compound yields was determined from the *YD* values (Fig. 2a). The *YD* value of H_2 increased and the *YD* values of CO and C_1–C_4 hydrocarbons decreased with rise in temperature. Co-pyrolysis at 700 °C had a positive impact on the H_2 yield, which was 1.3-fold of the theoretical yield, and negative effects on the production of CO and C_1–C_4 hydrocarbons. Hydrogen transfer from PE to biomass pyrolyzates suppresses the decarbonylation reaction [25,41]. The suppression of gaseous C_mH_n generation originates from gas–gas rather than gas–solid interactions [39]. Thus, the suppressive effect of the xylan and PE interaction on the gaseous C_mH_n yield was intensified with the rise in temperature in the present study.

Water (18.3–21.8 wt%) occupies approximately-one-third of the xylan liquid weight, and xylan dehydration is promoted at high temperatures (Table 1). The yield of the C_2–C_3 carbonyl compounds, represented mainly by ethanol and acetaldehyde, slightly decreased from 2.8 to 2.5 wt% with the increase in temperature. Whereas ethanol derives only from the ring opening and breakdown of the xylan main chain unit, the branched chain structure of the O-acetyl xylan unit can also generate some acetaldehyde [26]. More of the five-membered ring compounds were produced at 600–700 °C, owing to the ring opening of pyran followed by the cyclization reaction [26,27]. Other high-boiling-point polysaccharides could not be detected or had a low match degree in the GC/MS analysis [42,43]. The aliphatic hydrocarbons from PE pyrolysis were divided into gasoline (C_5–C_{10}), kerosene (C_{11}–C_{13}), diesel (C_{14}–C_{18}), heavy gas oil (C_{19}–C_{25}), and $C_{\geq 26}$ fractions according to carbon numbers [44]. Gasoline, diesel, and heavy gas oil were generated with a high yield, and their contents increased with the rise in PE pyrolysis temperature.

In co-pyrolysis, the oxygenated compound yield decreased, whereas that of liquid hydrocarbons accordingly increased with the increase in PE content in the mixture. The pyrolytic interactions significantly suppressed the production of the C_2–C_3 carbonyl compounds with the rise in temperature (Fig. 2b). PE blending further enhanced xylan dehydration, resulting in a 1.2–1.3-fold higher water content than that predicted by the theoretical yields, because polyolefin promotes dehydration of the hemicellulose-derived oxygenates [45]. The pyrolytic interaction at 600 °C inhibited the yields of five-membered ring compounds and phenols, in accordance with a previous study [46]. Furans can be converted into aromatic compounds by the Diels-Alder reaction followed by dehydration [29,41]. However, co-pyrolysis at high temperatures promoted production of these substances, corroborating a previous report [47]. In addition, the hydrocarbon oil ($C_{5-30}H_n$) yield was increased by

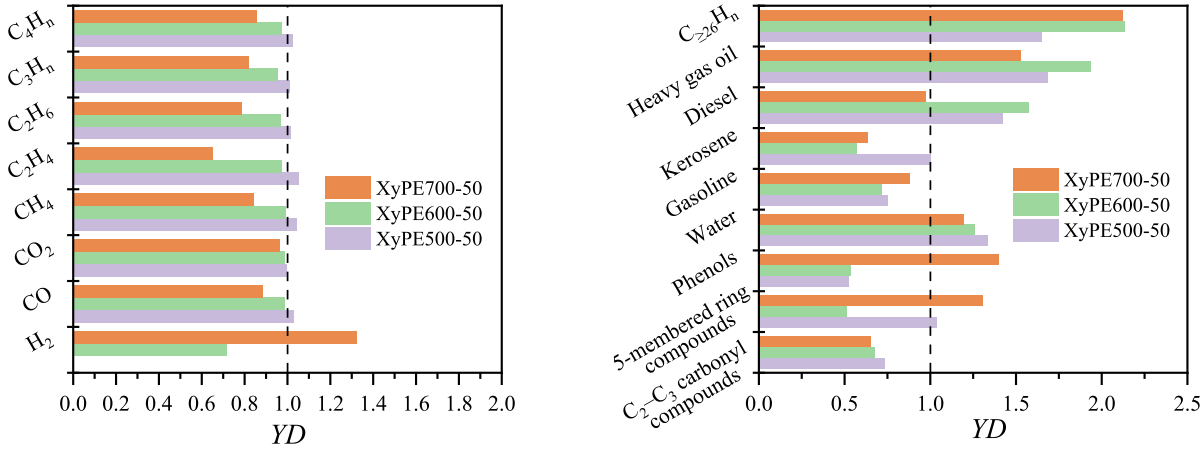

Fig. 2. Effects of temperature on the *YD* values of (a) gaseous and (b) liquid products from co-pyrolysis (xylan:PE = 50:50, w/w).

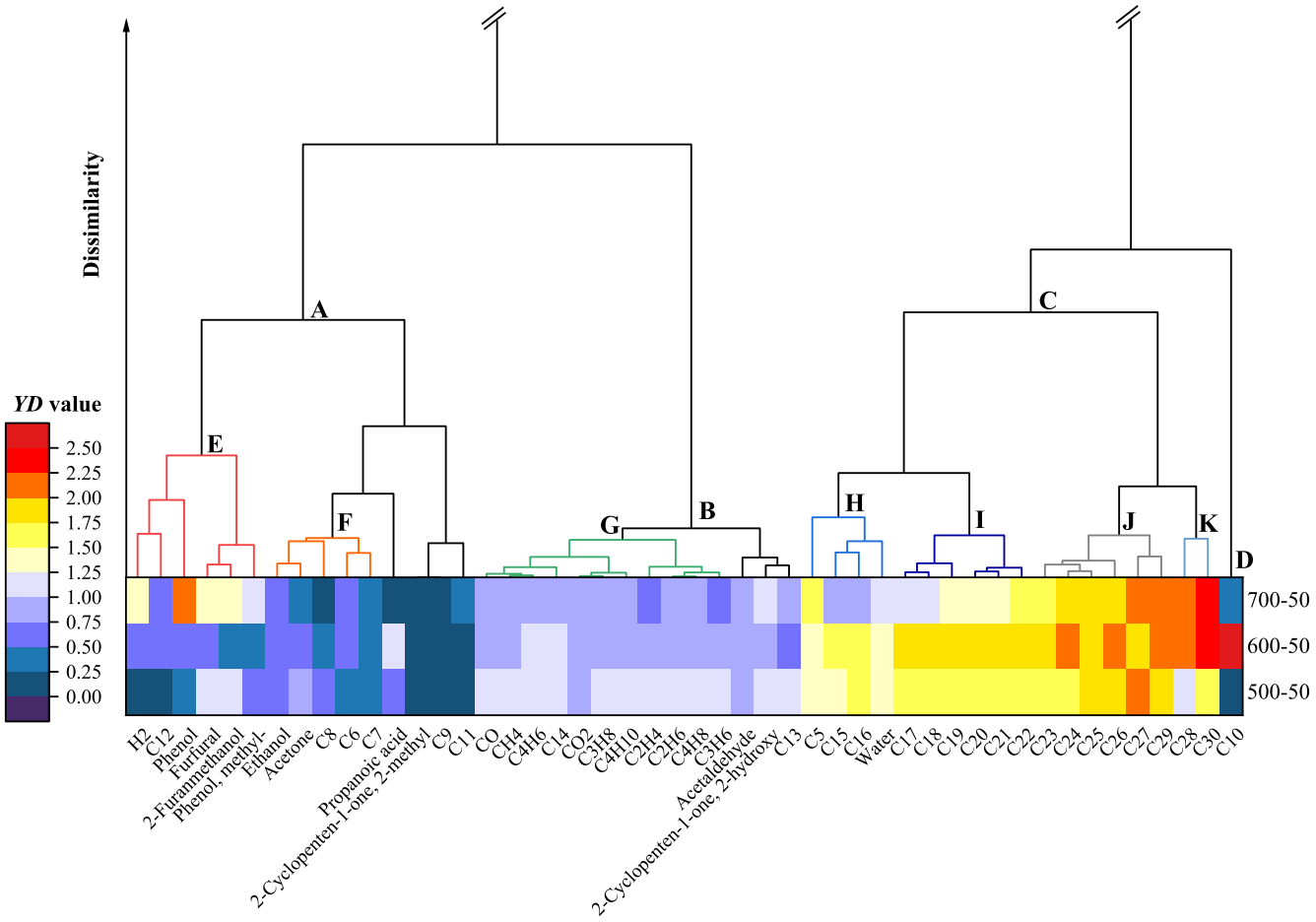

Fig. 3. Combination heat map with dendrogram obtained by HCA of *YD* values.

12–24 % after co-pyrolysis. In particular, the yields of heavy gas oil and $C_{\geq 26}$ fraction increased to 1.5–1.9-fold and 1.7–2.1-fold of theoretical values, respectively. These results are likely explained by the fact that oxygen-containing compounds from biomass oil promoted further chain scission of the linear long-chain radicals during PE pyrolysis and facilitated the transfer of the wax precursors into liquid fractions [29,38]. The enhancement of diesel and heavy gas oil production was the largest at 600 °C, as high temperatures increased the *YD* value of $C_{\geq 26}$ hydrocarbons.

Time courses of product emissions during co-pyrolysis were analyzed using the evolved gas analysis-MS (Fig. S4). The total ion chromatogram intensities of co-pyrolysis at different temperatures were higher than the theoretical ones, indicating more volatiles from co-pyrolysis were detected by MS. PE pyrolyzates enhanced xylan dehydration, which was verified by the fact that the peak at $m/z = 18$ was more intense after PE blending. The peak at $m/z = 280$–600 corresponds to the molecular ion of $C_{\geq 20}$ hydrocarbons; this peak significantly increased during co-pyrolysis, indicating that xylan pyrolyzates improved the heavy-fraction hydrocarbon formation by enhancing the decomposition of the PE-derived wax. The same phenomenon was also observed when we verified the results of the product recovery in the tube reactor.

3.2. Identification of synergies by using HCA

The potential pyrolytic synergies were identified using HCA (Fig. 3). The outcome "*YD* = 0" could be attributed to 0.00 wt% of pyrolyzate yield under certain conditions. All identified pyrolyzates were clearly classified into four major clusters based on *YD* values (A < B < C < D). Cluster A included H_2, xylan-derived liquid compounds, and some liquid hydrocarbons (C_6–C_9 and C_{11}–C_{12}). Cluster B comprised gaseous compounds, acetaldehyde, 2-hydroxy-2-cyclopenten-1-one, and $C_{13}H_n$. Water and most liquid hydrocarbons were classified into cluster C due to the enhanced yields after co-pyrolysis. Previous studies reported that fast co-pyrolysis of the biomass and PE improved the dehydration reaction and hydrocarbon oil production [38,47]. The $C_{10}H_n$ (cluster D) was highly different from other pyrolyzates, because the temperature significantly affected the pyrolytic interaction. In particular, co-pyrolysis at 600 °C resulted in a higher $C_{10}H_n$ yield than the theoretical value.

With regards to the sub-clusters, H_2, $C_{12}H_n$, phenols, furfural, and 2-furanmethanol were classified into cluster E, based on large *YD* values observed at high temperatures: co-pyrolysis at 700 °C improved the production of H_2, phenols, and some five-membered ring compounds. Cluster F indicated that the pyrolytic interactions suppressed the production of ethanol, acetone, and C_6–C_8 hydrocarbons. Xylan-derived carbonyl compounds are further decomposed under the action of hydrogen radicals [29]. Cluster G showed co-pyrolysis had similar synergies on the production of gaseous C_1–C_4 compounds, for which *YD* decreased with rise in temperature (*YD* < 1 at 700 °C). The C_5H_n, $C_{15}H_n$, $C_{16}H_n$, and water, classified into cluster H, were improved after co-pyrolysis at 500–600 °C. In addition, generation of the high molecular weight hydrocarbons was promoted by xylan blending, and they were organized into clusters I–K. Cluster I contained the C_{17}–C_{22} hydrocarbons, for which the extent of yield enhancement was as follows: 600 °C > 500 °C > 700 °C. The C_{23}–C_{27} and C_{29} hydrocarbons were classified into cluster J; the yields of these pyrolyzates were 1.7–2.2-fold of the theoretical values. Furthermore, the synergy promoted the yields of $C_{28}H_n$ and $C_{30}H_n$, included into cluster K, proportionally to the rise in

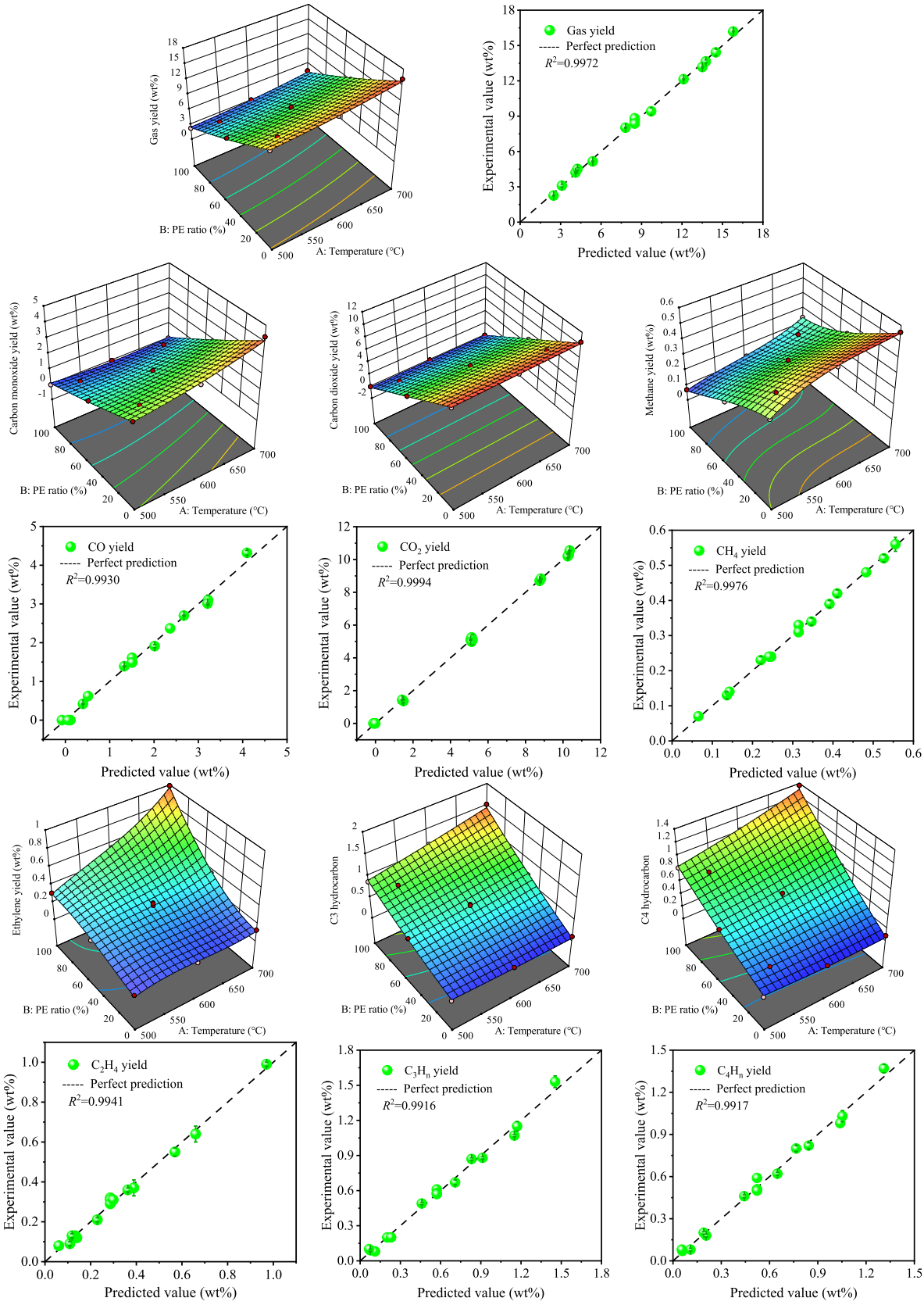

Fig. 4. Three-dimensional plots of the experimental yields of gaseous compounds (dots indicate yields at the corresponding PE ratios and temperatures) and response surfaces obtained by fitting to the models. Graphs near or below the three-dimensional plots illustrate correlations between predicted and experimental yields. The experimental values are closely similar to the predicted values along the perfect prediction line.

temperature. In summary, HCA divided the products with similar synergies into the same cluster and rapidly identified potential interactions of pyrolyzates with low yield.

3.3. RSM predicts pyrolyzate yields

3.3.1. Gaseous products

The product distribution models with low agreement are not discussed in the present study, because they had complicated yield variation or extremely low yield. The gas yield of co-pyrolysis presented a concave surface (Fig. 4). Therefore, the total gas yield was fitted to the quadratic model. Table 2 lists the detailed fitting polynomial equations of product yields. ANOVA showed that terms *A* and *B* significantly influenced the gas yield (Table S3). The high accuracy of the gas yield model was verified by the excellent agreement ($R^2 = 0.997$) of the predicted and experimental gas yields.

The CO yield increased at higher temperatures and lower PE ratios (Fig. 4). The suppressed interaction identified by HCA determined the concave curves based on the two-dimensional plot of CO yield versus PE ratio. Herein, the CO yield was well described by the quadratic model. PE ratio was the main influencing factor ($P < 0.001$) on the CO_2 yield that decreased at high PE ratios. The CO_2 yield of co-pyrolysis presented a flat variation and was fitted to the linear model, because the synergy had no significant influence on CO_2 production. The CH_4 and C_2H_4 yields increased with the rise in temperature, and higher PE content increased the C_2H_4 yield. The uneven two-dimensional plots of the CH_4/C_2H_4 yield versus PE ratio are likely explained by various synergies under different pyrolysis conditions. Herein, the CH_4 and C_2H_4 yields presented uneven surfaces, which were well described by cubic models. Their complicated yield distributions were also observed after co-pyrolysis of cellulose and PE [32]. The C_3 and C_4 hydrocarbon yields increased with the increases in temperature and PE ratio. The inhibited synergies determined their concave distribution that could be described by the quadratic model. Furthermore, the ANOVA parameters of gaseous compound distributions reflected the reliability of the response models (Table S3). The predicted yields were close to the experimental ones with R^2 values >0.991, verifying the accuracy of the model for gaseous pyrolyzates.

3.3.2. Liquid products

The liquid yield increased at high pyrolysis temperatures and low PE blending ratios (Fig. 5). The convex curves in the two-dimensional plot of the liquid yield versus PE ratio are likely explained by the enhanced impact of co-pyrolysis on liquid production. Thus, the liquid yield presented a convex surface variation, fitting to the quadratic model mathematically expressed in Table 2. ANOVA showed that the liquid yield was significantly influenced by terms *A* and *B* (Table S4). The high correlation ($R^2 = 0.994$) between the predicted and experimental liquid yields verified the model prediction accuracy.

Fig. 5 shows that the PE ratio was the main factor ($P < 0.001$) influencing the ethanol and acetaldehyde yields compared with pyrolysis temperature ($P > 0.05$). The two-dimensional plot of the carbonyl compound yield versus PE ratio showed a concave curve variation because HCA identified the suppressed interaction of co-pyrolysis. Accordingly, the ethanol and acetaldehyde yields presented concave surfaces that were well described by quadratic models. The hydrocarbon oil yield remarkably increased with the increases in temperature and PE ratio. The convex curves in the two-dimensional plot of the liquid hydrocarbon yield versus PE ratio can be attributed to the stronger effect of the synergy on liquid hydrocarbon generation. Herein, the hydrocarbon oil yield of co-pyrolysis showed a convex surface variation that was fitted to the quadratic model. The gasoline generation increased with the increases in temperature and PE ratio. The inhibited synergies determined the concave surface of gasoline distribution, which was well described by the quadratic model. All fitted liquid compound yield models were reliable, considering that their *P*-values were below 0.05. The highly precise fitting ($R^2 > 0.949$) indicated that the distribution models of liquid compounds established by RSM can be applied for accurate yield prediction.

3.3.3. Solid and char

The solid is mainly derived from PE pyrolysis, and its yield decreased at high temperatures and low PE blending ratios (Fig. 6). The concave two-dimensional curves of the solid yield versus PE ratio are explained by the fact that xylan pyrolyzates suppressed the solid deposition by decomposing PE-derived wax into liquid hydrocarbons. The solid yield showed a non-linear variation with the rise in temperature. Thus, the distribution of the solid yield from co-pyrolysis presented a convex surface that was fitted by the quadratic model, and its polynomial equation is listed in Table 2. ANOVA showed that the solid yield was significantly influenced by terms *A*, *B*, *AB*, and B^2 (Table S5). The established model accurately predicted the solid yield in the subsequent experiments ($R^2 = 0.998$).

The char yield decreased with the increases in temperature and PE ratio. In the two-dimensional plot of char yield versus PE ratio, the experimental char yields were lower than the theoretically calculated ones, which was also verified by *YD* values in Section 3.1. Accordingly, the yield of char from co-pyrolysis presented a concave surface variation

Table 2
Polynomial equations fitting of product yields.

Composition	Regression model	Fitted equation (*A* is pyrolysis temperature and *B* is PE proportion.)
Gas	Quadratic	$Y_{gas} = 18.13776–0.022244A-0.118939B-0.000013AB + 0.000027A^2 + 0.000125B^2$
CO	Quadratic	$Y_{CO} = 4.91622–0.012772A + 0.008694B-0.000074AB + 0.000017A^2 + 0.000026B^2$
CO_2	Linear	$Y_{CO2} = 10.00881 + 0.000496A-0.103664B$
CH_4	Cubic	$Y_{CH4} = -7.61329 + 0.036418A + 0.029427B-0.000097AB-0.000054A^2-0.000100B^2 + 7.0 \times 10^{-8}A^2B + 1.4 \times 10^{-7}AB^2 + 2.73109 \times 10^{-8}A^3 + 1.52533 \times 10^{-7}B^3$
C_2H_4	Cubic	$Y_{C2H4} = -12.15944 + 0.060684A + 0.038135B-0.000112AB-0.000100A^2-0.000190B^2 + 8.5 \times 10^{-8}A^2B + 4.1 \times 10^{-7}AB^2 + 5.42717 \times 10^{-8}A^3-2.29441 \times 10^{-7}B^3$
C_3H_n	Quadratic	$Y_{C3Hn} = 0.661938–0.001732A-0.008708 + 0.000029AB + 1.25985 \times 10^{-6}A^2 + 0.000021B^2$
C_4H_n	Quadratic	$Y_{C4Hn} = 1.07085–0.003105A-0.007025 + 0.000026AB + 2.36195 \times 10^{-6}A^2 + 0.000013B^2$
Liquid	Quadratic	$Y_{liquid} = 79.75687–0.123490A-0.497425B + 0.000214AB + 0.000132A^2-0.000400B^2$
Ethanol	Quadratic	$Y_{ethanol} = 3.08186–0.004692A-0.029523B + 7.18855 \times 10^{-6}AB + 3.18507 \times 10^{-6}A^2 + 0.000112B^2$
Acetaldehyde	Quadratic	$Y_{acetaldehyde} = 2.20143–0.003342A-0.020487B + 0.000012AB + 2.01610 \times 10^{-6}A^2 + 0.000040B^2$
Hydrocarbon oil	Quadratic	$Y_{hydrocarbon\ oil} = 29.46163–0.098049A-0.233416B + 0.000584AB + 0.000081A^2-0.000305B^2$
Gasoline	Quadratic	$Y_{gasoline} = 10.01401–0.031860A-0.059143B + 0.000116AB + 0.000026A^2 + 0.000135B^2$
Solid	Quadratic	$Y_{solid} = -39.29605 + 0.147704A + 1.03425B-0.000651AB-0.000131A^2 + 0.001197B^2$
Char	Quadratic	$Y_{char} = 20.94121 + 0.037517A-0.466682B + 0.000353AB-0.000060A^2 + 0.000410B^2$

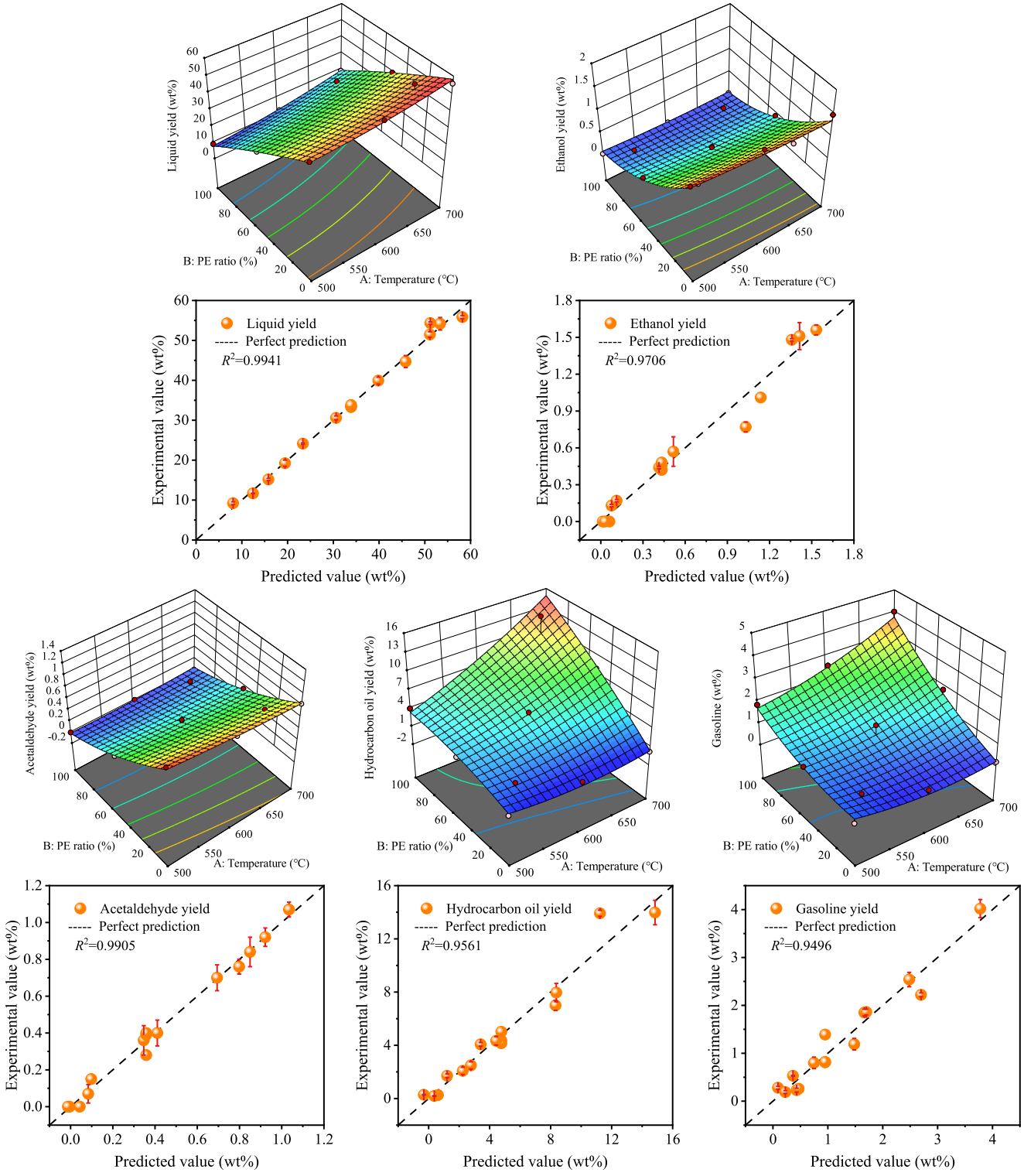

Fig. 5. Three-dimensional plots of the experimental yields of liquid compounds (dots indicate yields at the corresponding PE ratios and temperatures) and response surfaces obtained by fitting to the models. Graphs below the three-dimensional plots illustrate correlations between predicted versus experimental yields. The experiment values are closely similar to the predicted values along the perfect prediction line.

and was well described by the quadratic model. ANOVA verified the reliability of the char distribution model, where *A*, *B*, and *AB* were the major terms affecting the char yield. The close agreement ($R^2 = 0.995$) between predicted and experimental yields showed the excellent prediction potential of the RSM model.

4. Conclusions

In the present work, a novel strategy was proposed to rapidly identify pyrolytic interactions and predict yields of products generated by xylan and polyethylene co-pyrolysis. HCA classified pyrolyzates with similar *YD* values into the same cluster, making up for the deficiencies of RSM in

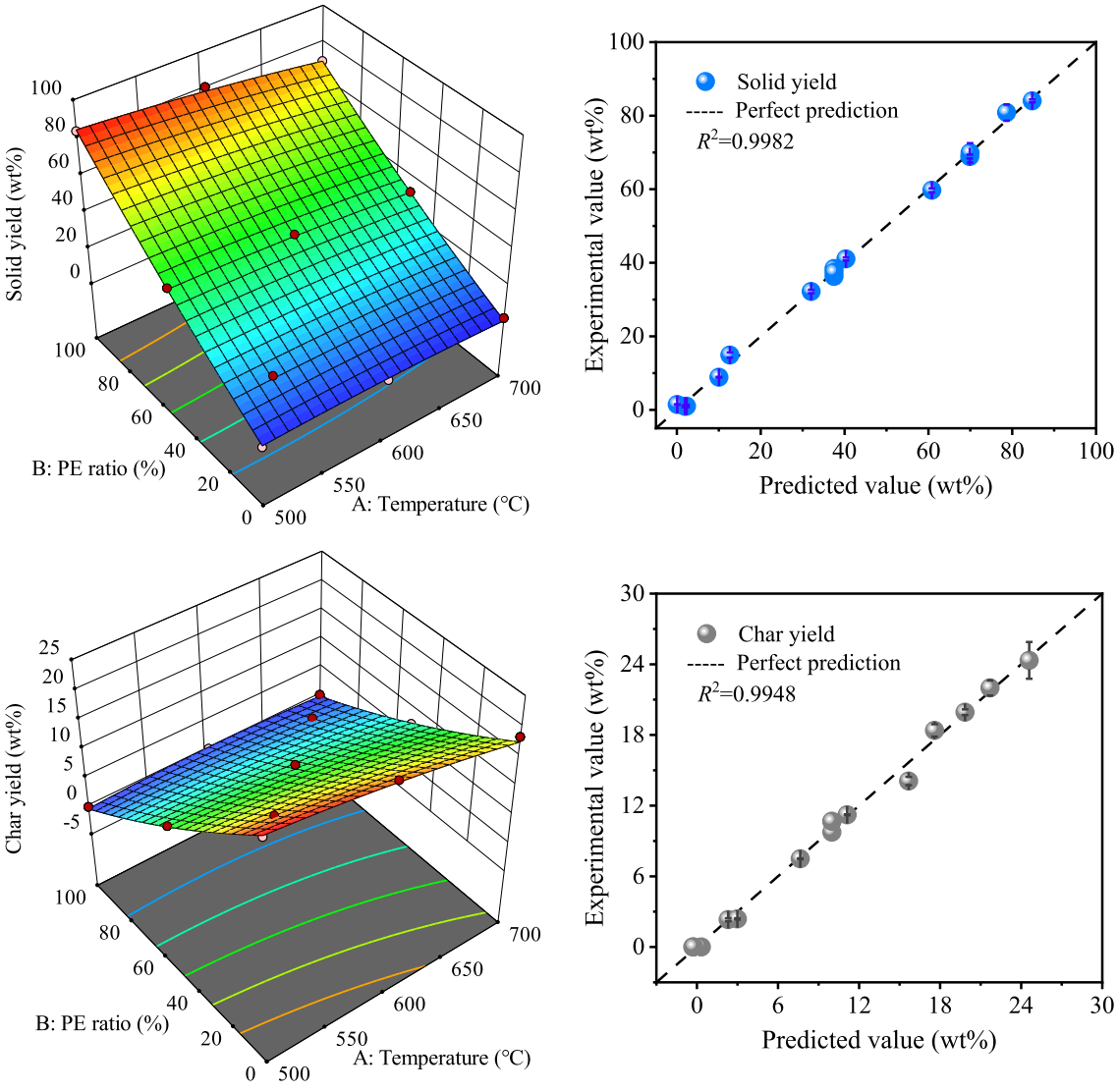

Fig. 6. Three-dimensional plots of experimental yields of solid and char (dots indicate yields at the corresponding PE ratios and temperatures) and response surfaces obtained by fitting to the model. Graphs near the three-dimensional plots illustrate predicted versus experimental yields. The experimental values are closely similar to the predicted values along the perfect prediction line.

the synergy analysis of low-yield products. We found that PE intermediates enhanced the dehydration of xylan-derived oxygenates, and xylan pyrolyzates promoted the further breakdown of the PE-derived wax into high carbon number hydrocarbons. The quadratic, cubic, and linear RSM models of product distributions were established according to the synergies, which accurately predicted specific pyrolyzate yields in addition to total gas, liquid, and char yields. Although the utility of HCA and RSM was investigated based on the case of xylan and PE co-pyrolysis, this strategy may be extended to the interaction analysis and product prediction of the co-treatment process. The results of our study may help to maximize the efficiency of conversion of the biomass and plastic waste, as carbon and hydrogen resources, into value-added chemical feedstocks.

CRediT authorship contribution statement

Shengyu Xie: Investigation, Formal analysis, Writing - Original Draft, Writing - Review & Editing. **Shogo Kumagai:** Conceptualization, Writing - Original Draft, Writing - Review & Editing, Supervision, Project administration. **Naomichi Takahashi:** Formal analysis, Writing - Review & Editing. **Tomohito Kameda:** Writing - Review & Editing. **Yuko Saito:** Writing - Review & Editing. **Toshiaki Yoshioka:** Writing - Review & Editing.

Declaration of Competing Interest

The authors declare that they have no known competing financial interests or personal relationships that could have appeared to influence the work reported in this paper.

Data availability

Data will be made available on request.

Acknowledgements

This work was supported by the JST FOREST Program (Grant number: JPMJFR206U). Shengyu Xie was supported by the Chinese Scholarship Council (Grant number: CSC201904910424).

Appendix A. Supplementary data

Supplementary data to this article can be found online at https://doi.org/10.1016/j.cej.2022.139958.

References

[1] R. Geyer, J.R. Jambeck, K.L. Law, Production, use, and fate of all plastics ever made, Sci. Adv. 3 (7) (2017) e1700782.

[2] M. Carus, A. Eder, L. Dammer, H. Korte, L. Scholz, R. Essel, E. Breitmayer, M. Barth, Wood-plastic composites (WPC) and natural fibre composites (NFC), Nova-Institute, Hürth, Germany, 2015, pp. 1–16.

[3] G. Lopez, M. Artetxe, M. Amutio, J. Bilbao, M. Olazar, Thermochemical routes for the valorization of waste polyolefinic plastics to produce fuels and chemicals. A review, Renew Sust. Energ. Rev. 73 (2017) 346–368, https://doi.org/10.1016/j.rser.2017.01.142.

[4] S. Kumagai, T. Yoshioka, Chemical feedstock recovery from hard-to-recycle plastics through pyrolysis-based approaches and pyrolysis-gas chromatography, Bull. Chem. Soc. Jpn. 94 (10) (2021) 2370–2380, https://doi.org/10.1246/bcsj.20210219.

[5] A. Awasthi, G. Singh, V. Dhyani, J. Kumar, Y.S. Reddy, V.P. Adarsh, A. Puthiyamadam, K.K. Mullepureddy, R.K. Sukumaran, S.B. Ummalyma, D. Sahoo, T. Bhaskar, Co-pyrolysis of phumdi and para grass biomass from Loktak Lake, Bioresour. Technol. 285 (2019), 121308, https://doi.org/10.1016/j.biortech.2019.03.147.

[6] C. Wu, P.T. Williams, Pyrolysis–gasification of plastics, mixed plastics and real-world plastic waste with and without Ni–Mg–Al catalyst, Fuel 89 (10) (2010) 3022–3032, https://doi.org/10.1016/j.fuel.2010.05.032.

[7] Y.-K. Park, J.S. Jung, J. Jae, S.B. Hong, A. Watanabe, Y.-M. Kim, Catalytic fast pyrolysis of wood plastic composite over microporous zeolites, Chem. Eng. J. 377 (2019), 119742, https://doi.org/10.1016/j.cej.2018.08.128.

[8] C. Ma, S. Kumagai, Y. Saito, T. Kameda, T. Yoshioka, Enhanced production of phenol and debromination by co-pyrolysis of the non-metallic fraction of printed circuit boards and waste tires, Green Chem. 23 (17) (2021) 6392–6404, https://doi.org/10.1039/D1GC01176F.

[9] A. Demirbas, Competitive liquid biofuels from biomass, Appl. Energy 88 (1) (2011) 17–28, https://doi.org/10.1016/j.apenergy.2010.07.016.

[10] O. Sanahuja-Parejo, A. Veses, M.V. Navarro, J.M. López, R. Murillo, M.S. Callén, T. García, Drop-in biofuels from the co-pyrolysis of grape seeds and polystyrene, Chem. Eng. J. 377 (2019), 120246, https://doi.org/10.1016/j.cej.2018.10.183.

[11] F. Nardella, S. Bellavia, M. Mattonai, E. Ribechini, Co-pyrolysis of biomass and plastic: synergistic effects and estimation of elemental composition of pyrolysis oil by analytical pyrolysis–gas chromatography/mass spectrometry, Bioresour. Technol. 354 (2022), 127170, https://doi.org/10.1016/j.biortech.2022.127170.

[12] X. Li, J. Li, G. Zhou, Y. Feng, Y. Wang, G. Yu, S. Deng, J. Huang, B. Wang, Enhancing the production of renewable petrochemicals by co-feeding of biomass with plastics in catalytic fast pyrolysis with ZSM-5 zeolites, Appl. Catal. A Gen. 481 (2014) 173–182, https://doi.org/10.1016/j.apcata.2014.05.015.

[13] H. Hassan, J.K. Lim, B.H. Hameed, Recent progress on biomass co-pyrolysis conversion into high-quality bio-oil, Bioresour. Technol. 221 (2016) 645–655, https://doi.org/10.1016/j.biortech.2016.09.026.

[14] W.A. Wan Mahari, E. Azwar, S.Y. Foong, A. Ahmed, W. Peng, M. Tabatabaei, M. Aghbashlo, Y.-K. Park, C. Sonne, S.S. Lam, Valorization of municipal wastes using co-pyrolysis for green energy production, energy security, and environmental sustainability: a review, Chem. Eng. J. 421 (2021), 129749, https://doi.org/10.1016/j.cej.2021.129749.

[15] D.K. Ojha, R. Vinu, Chapter 12 - Copyrolysis of Lignocellulosic Biomass With Waste Plastics for Resource Recovery, in: T. Bhaskar, A. Pandey, S.V. Mohan, D.-J. Lee, S. K. Khanal (Eds.), Waste Biorefinery, Elsevier, 2018, pp. 349–391.

[16] B.B. Uzoejinwa, X. He, S. Wang, A. El-Fatah Abomohra, Y. Hu, Q. Wang, Co-pyrolysis of biomass and waste plastics as a thermochemical conversion technology for high-grade biofuel production: recent progress and future directions elsewhere worldwide, Energy Convers. Manage. 163 (2018) 468–492, https://doi.org/10.1016/j.enconman.2018.02.004.

[17] Z. Wang, K.G. Burra, T. Lei, A.K. Gupta, Co-pyrolysis of waste plastic and solid biomass for synergistic production of biofuels and chemicals-A review, Prog. Energy Combust. Sci. 84 (2021), 100899, https://doi.org/10.1016/j.pecs.2020.100899.

[18] G. Lopez, A. Erkiaga, M. Amutio, J. Bilbao, M. Olazar, Effect of polyethylene co-feeding in the steam gasification of biomass in a conical spouted bed reactor, Fuel 153 (2015) 393–401, https://doi.org/10.1016/j.fuel.2015.03.006.

[19] S. Kumagai, T. Yoshioka, Latest trends in pyrolysis gas chromatography for analytical and applied pyrolysis of plastics, Anal. Sci. 37 (1) (2021) 145–157, https://doi.org/10.2116/analsci.20SAR04.

[20] Y. Xue, S. Zhou, R.C. Brown, A. Kelkar, X. Bai, Fast pyrolysis of biomass and waste plastic in a fluidized bed reactor, Fuel 156 (2015) 40–46, https://doi.org/10.1016/j.fuel.2015.04.033.

[21] H. Hassan, B.H. Hameed, J.K. Lim, Co-pyrolysis of sugarcane bagasse and waste high-density polyethylene: synergistic effect and product distributions, Energy 191 (2020), 116545, https://doi.org/10.1016/j.energy.2019.116545.

[22] C. Ma, S. Xie, S. Kumagai, Y. Takahashi, Y. Saito, T. Kameda, T. Yoshioka, Synergistic effects during co-pyrolysis of milled wood lignin and polyolefins at the gas phase and liquid/solid phase contacting modes, Chem. Eng. J. 431 (2022), 134030, https://doi.org/10.1016/j.cej.2021.134030.

[23] S. Kumagai, K. Fujita, T. Kameda, T. Yoshioka, Interactions of beech wood–polyethylene mixtures during co-pyrolysis, J. Anal. Appl. Pyrolysis 122 (2016) 531–540, https://doi.org/10.1016/j.jaap.2016.08.012.

[24] S. Kumagai, K. Fujita, Y. Takahashi, Y. Nakai, T. Kameda, Y. Saito, T. Yoshioka, Beech Wood Pyrolysis in Polyethylene Melt as a Means of Enhancing Levoglucosan and Methoxyphenol Production, Sci. Rep. 9 (1) (2019) 1955, https://doi.org/10.1038/s41598-018-37146-w.

[25] S. Xie, C. Ma, S. Kumagai, Y. Takahashi, T. Kameda, Y. Saito, T. Yoshioka, Improving levoglucosan and hydrocarbon production through gas-phase synergy during cellulose and polyolefin co-pyrolysis, Sustain. Energ. Fuels 6 (6) (2022) 1469–1478, https://doi.org/10.1039/D1SE01836A.

[26] D.K. Shen, S. Gu, A.V. Bridgwater, Study on the pyrolytic behaviour of xylan-based hemicellulose using TG–FTIR and Py–GC–FTIR, J. Anal. Appl. Pyrolysis 87 (2) (2010) 199–206, https://doi.org/10.1016/j.jaap.2009.12.001.

[27] D.O. Usino, Supriyanto, P. Ylitervo, A. Pettersson, T. Richards, Influence of temperature and time on initial pyrolysis of cellulose and xylan, J. Anal. Appl. Pyrolysis 147 (2020) 104782, https://doi.org/10.1016/j.jaap.2020.104782.

[28] J. Wang, M. Asmadi, H. Kawamoto, The effect of uronic acid moieties on xylan pyrolysis, J. Anal. Appl. Pyrolysis 136 (2018) 215–221, https://doi.org/10.1016/j.jaap.2018.10.002.

[29] J. Gu, H. Fan, Y. Wang, Y. Zhang, H. Yuan, Y. Chen, Co-pyrolysis of xylan and high-density polyethylene: product distribution and synergistic effects, Fuel 267 (2020), 116896, https://doi.org/10.1016/j.fuel.2019.116896.

[30] C. Dorado, C.A. Mullen, A.A. Boateng, H-ZSM5 Catalyzed Co-Pyrolysis of Biomass and Plastics, ACS Sustain. Chem. Eng. 2 (2) (2014) 301–311, https://doi.org/10.1021/sc400354g.

[31] Y. Zheng, J. Wang, C. Liu, X. Lin, Y. Lu, W. Li, Z. Zheng, Enhancing the aromatic hydrocarbon yield from the catalytic copyrolysis of xylan and LDPE with a dual-catalytic-stage combined CaO/HZSM-5 catalyst, J. Energy Inst. 93 (5) (2020) 1833–1847, https://doi.org/10.1016/j.joei.2020.03.014.

[32] S. Xie, S. Kumagai, T. Kameda, Y. Saito, T. Yoshioka, Prediction of pyrolyzate yields by response surface methodology: a case study of cellulose and polyethylene co-pyrolysis, Bioresour. Technol. 337 (2021), 125435, https://doi.org/10.1016/j.biortech.2021.125435.

[33] F. Nielsen, Hierarchical Clustering, in: Introduction to HPC With MPI for Data Science, Springer International Publishing, Cham, 2016, pp. 195–211, https://doi.org/10.1007/978-3-319-21903-5_8.

[34] S. Kumagai, A. Matsukami, F. Kabashima, M. Sakurai, M. Kanai, T. Kameda, Y. Saito, T. Yoshioka, Combining pyrolysis–two-dimensional gas chromatography–time-of-flight mass spectrometry with hierarchical cluster analysis for rapid identification of pyrolytic interactions: case study of co-pyrolysis of PVC and biomass components, Process Saf. Environ. Protect. 143 (2020) 91–100, https://doi.org/10.1016/j.psep.2020.06.036.

[35] J. Grabowski, A. Smoliński, The application of hierarchical clustering to analyzing ashes from the combustion of wood pellets mixed with waste materials, Environ. Pollut. 276 (2021), 116766, https://doi.org/10.1016/j.envpol.2021.116766.

[36] N. Howaniec, A. Smoliński, Influence of fuel blend ash components on steam co-gasification of coal and biomass – chemometric study, Energy 78 (2014) 814–825, https://doi.org/10.1016/j.energy.2014.10.076.

[37] J.H. Ward, Hierarchical grouping to optimize an objective function, J. Am. Stat. Assoc. 58 (301) (1963) 236–244, https://doi.org/10.1080/01621459.1963.10500845.

[38] K. Kasataka, S. Kumagai, T. Kameda, Y. Saito, T. Yoshioka, Enhancement of gasification and liquefaction during fast co-pyrolysis of cedar wood and polyethylene through control of synergistic interactions, Bioresour. Technol. Rep. 11 (2020), 100431, https://doi.org/10.1016/j.biteb.2020.100431.

[39] X. Liu, K.G. Burra, Z. Wang, J. Li, D. Che, A.K. Gupta, On deconvolution for understanding synergistic effects in co-pyrolysis of pinewood and polypropylene, Appl. Energy 279 (2020), 115811, https://doi.org/10.1016/j.apenergy.2020.115811.

[40] H. Yang, R. Yan, H. Chen, D.H. Lee, C. Zheng, Characteristics of hemicellulose, cellulose and lignin pyrolysis, Fuel 86 (12) (2007) 1781–1788, https://doi.org/10.1016/j.fuel.2006.12.013.

[41] Y. Xue, A. Kelkar, X. Bai, Catalytic co-pyrolysis of biomass and polyethylene in a tandem micropyrolyzer, Fuel 166 (2016) 227–236, https://doi.org/10.1016/j.fuel.2015.10.125.

[42] P.R. Patwardhan, R.C. Brown, B.H. Shanks, Product distribution from the fast pyrolysis of hemicellulose, Chem. Sus. Chem. 4 (5) (2011) 636–643, https://doi.org/10.1002/cssc.201000425.

[43] S. Wang, B. Ru, H. Lin, W. Sun, Pyrolysis behaviors of four O-acetyl-preserved hemicelluloses isolated from hardwoods and softwoods, Fuel 150 (2015) 243–251, https://doi.org/10.1016/j.fuel.2015.02.045.

[44] R.C. Selley, S.A. Sonnenberg, Chapter 2 - The Physical and Chemical Properties of Petroleum, in: R.C. Selley, S.A. Sonnenberg (Eds.), Elements of Petroleum Geology (Third Edition), Academic Press, Boston, 2015, pp. 13–39.

[45] X. Lin, Z. Zhang, Q. Wang, J. Sun, Interactions between biomass-derived components and polypropylene during wood–plastic composite pyrolysis, Biomass Convers. Biorefinery 12 (8) (2022) 3345–3357.

[46] J. Yang, J. Rizkiana, W.B. Widayatno, S. Karnjanakom, M. Kaewpanha, X. Hao, A. Abudula, G. Guan, Fast co-pyrolysis of low density polyethylene and biomass residue for oil production, Energy Convers. Manage. 120 (2016) 422–429, https://doi.org/10.1016/j.enconman.2016.05.008.

[47] S. Kumagai, K. Fujita, Y. Takahashi, T. Kameda, Y. Saito, T. Yoshioka, Impacts of pyrolytic interactions during the Co-pyrolysis of biomass/plastic: synergies in lignocellulose-polyethylene system, J. Jpn. Inst. Energy 98 (9) (2019) 202–219, https://doi.org/10.3775/jie.98.202.